On understanding the microstructure of SiC/SiC Ceramic Matrix Composites (CMCs) after a material removal process

O. Gavalda Diaz[a], D.A. Axinte[a,*], P. Butler-Smith[a], D. Novovic[b]

[a] *Rolls-Royce University Technology Centre in Manufacturing and On-Wing Technology, Faculty of Engineering, University of Nottingham, NG8 1BB, UK*
[b] *Manufacturing Technology, Rolls-Royce Plc, DE24 8ER, UK*

Abstract

The unique material nature (e.g. hard, brittle, heterogeneous and orthotropic) of SiC-based Ceramic Matrix Composites (CMCs) highly affects the outcomes of machining process by inducing high thermo-mechanical loads during material removal. This can result in severe material damage which in turn causes a reduction of the in-service life of critical structural ceramic components (such as in aero-engines or nuclear reactors). In this study, the phenomenon by which the material removal mechanism during drilling influences the CMC surface integrity are discussed by characterising the fracture and deformation phenomena on the CMC's constituents - i.e. SiC and Si materials. Moreover, the strain induced to the surface, together with the changes in chemical composition are characterised via micro Raman spectroscopy and related to the principles of residual stresses upon cutting. This results in a novel understanding of the material removal process that governs cutting of SiC-based CMCs while emphasising how the different microstructure, morphology and nature of ceramics behave under the same cutting conditions. This study has therefore led to a comprehension of how the microstructure of complex hierarchical ceramic materials such as SiC/SiC CMCs is affected by a mechanical cutting process and opens avenues to understand the structure damage under other machining operations (e.g. milling, grinding).

Keywords: Ceramic Matrix Composites, Microstructure, Residual stresses, Material removal mechanism, Machining

*Corresponding author
Email address: Dragos.Axinte@nottingham.ac.uk (D.A. Axinte)

1. Introduction

Silicon Carbide (SiC) Ceramic Matrix Composites (CMCs) have been an important research field within the aerospace industry in recent years. SiC matrices reinforced with SiC fibres allow for an improved in-service behaviour, maintaining their high strength at temperatures up to 1250°C, an increase of about 150°C compared to Nickel-based superalloys. Is therefore anticipated that in high temperature structural applications (e.g. aerospace or nuclear) where re-usability is a key factor, the SiC/SiC CMC structures are one of the more promising groups of material candidates [1].

The SiC matrix can be manufactured/processed by three main routes [2]: pyrolysis of a SiC pre-ceramic precursors [3, 4], chemical vapour infiltration (CVI) [5, 6] and melt infiltration (MI) [7]. In terms of SiC fibres, three main manufacturers found in the market are Nippon Carbon, COI Ceramics and Ube ind, producing the trade-marks Hi-Nicalon (Type-S), Sylramic (iBN) and Tyranno SA3 respectively, where the elemental composition of the precursors and the maximum production temperature varies [8]. The melt infiltration method in SiC-based CMCs has been established as a reference method for the aerospace industry as a fully-dense matrix can be achieved [7, 9]. In these materials, a Boron Nitride (BN) or a Pyrolytic Carbon (PyC) coating is deposited around fibres to produce an improved mechanical behaviour by creating weak interfaces which bridge the crack propagations [10, 11]. Moreover, it has been reported in the literature [12, 13] that in aerospace applications, where this interface can be exposed to severe environments (due to the fibre-matrix bridging mechanism), BN coatings could improve the corrosion resistance. Further improvements in CMC manufacturing for the aerospace industry aimed to reduce the porosity and protecting the fibres-interface integrity during the matrix formation. For these reasons, several CMC manufacturers added an extra step prior to the melt infiltration process which consists of producing a SiC or Si_3N_4 coating by Chemical Vapor Infiltration (CVI) [7, 14], resulting in a combined CVI-MI process for the manufacturing of SiC-based CMCs.

To characterise the manufacturing process, Raman spectroscopy has been shown to give precise results in measuring the point-by-point strain by quantifying the peak shift [15]. Consequently, a few authors have focused their work on characterising the CMC forming processes by understanding the residual stresses and chemical composition of

the reinforcement structure and the matrix [16]. Wing et al. [9, 17] reported that in a melt infiltrated matrix (forming a SiC-Si), the Si phase suffers from compressive residual stresses while the SiC is exposed to tensile microstresses caused by the difference in Coefficient of Thermal Expansion (CTE) between the Si and SiC. Gouadec et al. [18] studied the induced residual stresses in uncoated and BN coated Hi-Nicalon fibres, finding compressive stresses in the fibres when embedded a Celsian matrix. On the other hand, Knauf [19] reported that in a SiC/SiC CMC manufactured via CVI-MI, fibres do not suffer any significant induced residual stress. Moreover, Knauf [20] proposed a novel approach which characterises the residual stresses in a MI SiC matrix with B-doped Si, which concludes that the Si regions are under compression while the SiC particles are under tensile residual stresses.

It is therefore clear that the stressed condition in which CMCs result after the primary manufacturing has been recently studied as a method of characterising and understanding the matrix formation process. Nevertheless, the increasing demand of CMCs in high-value and complex parts for the aerospace and nuclear industries has also created the need for using conventional machining processes (i.e. drilling, milling, grinding) with the aim of obtaining the final shape and/or smooth surfaces. Microstructural investigations of the machined surface in metals such as Carbon steels [21], Nickel-based superalloys [22, 23] or monolithic ceramics such as RB SiC [24] have been reported in the literature. Nonetheless, when it comes to understand the material damage after a mechanical removal process in difficult-to-machine SiC-based CMCs, the research background is, to the authors knowledge, almost non-existent. The understanding of the machined surface of CMCs from the point of view of microstructural changes is challenging due to the initial prestressed condition and different brittle-ductile nature of the various constituents. Moreover, several specific engineered interfaces (e.g. between fibres and CVI coatings) are created which can absorb machining energy by cracking or debonding. Ghosh et al. [25, 26] studied the surface integrity after a scratch test in a particle ceramic ZrB_2-SiC showing that both microplasticity and microcracking are dominant mechanisms during the process and measured tensile residual stresses in the SiC particles. However, these studies are far from being relevant to machining. Gavalda and Axinte [27] reported, by using the orthogonal cutting scheme, that different fracture mechanisms occur in a CMC

depending on the fibre orientation, however the effect on the surface integrity was not characterised. As shown in Fig.1, in the specific case of drilling of SiC-based CMCs, a combination of the cutting scenarios occur in a closed environment (within the hole) where high thermomechanical loads are formed [28] and which can be very detrimental for the machined surface. From the cutting mechanisms showed in Fig.1 it could be commented that parallel (Fig.1a) and transverse (Fig.1b) fibres are the main fundamental scenarios to study the removal process as they represent the orthotropic directions of the material [27]. Furthermore, in the transverse cutting scenario, the fibres need to be fractured through their preferential axis (with higher values of translaminar than interlaminar fracture toughness), leading to a more complex fracture and deformation mechanisms which do not occur in the parallel fibres scenario where a simpler debonding mechanism is the dominant removal mechanism [27].

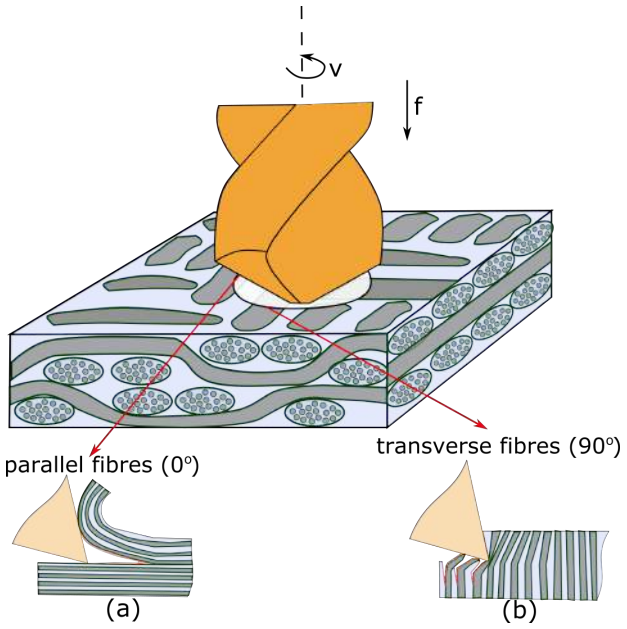

Figure 1: Material response diagram to the drilling of orthotropic materials with a schematic of (a) fibres placed parallel to the cutting speed (0°) and (b) fibres placed perpendicular to the cutting speed (90°).

In this study, an explanation of the thermomechanics by which the damage is incurred to the CMC structure by putting in evidence their fracture morphology, induced strain and change in composition is presented. This is then related to the theoretical

understanding of residual stresses upon cutting and how the different microstructures and morphologies found within a SiC-based CMC are affected by a mechanical removal process.

2. Experimental procedure

Because of its hard, heterogeneous, anisotropic and brittle nature, SiC/SiC materials can be considered as one of the most difficult to machine CMCs. Drilling experiments were performed in a CVI-MI SiC/SiC with Hi-Nicalon fibres in a woven architecture of a 5 harness satin (5HS) using a 5 mm diamond coated twist drill. As aforementioned, to protect the fibres and improve the mechanical and chemical performance of the CMC, a CVI BN followed by a CVI SiC coating was employed during the manufacturing process (as similarly explained in [19]) resulting in the morphology shown in Fig.2b. Preoptimised cutting parameters (f = 2 mm/min and v = 3000 rpm) were used to drill the CMC which anyway resulted in high mechanical and thermal loads, as explained in [28].

To allow for the observation of the machined surface, the drilled holes were sectioned along the height (section A-A in Fig.2a) by abrasive waterjet cutting at reduced feed rates to avoid any delamination. The sectioned "as-machined" samples were analysed in cross section after polishing (red surface in Fig.2c) and without polishing (yellow surface in Fig.2c). Furthermore, to gather the reference information from the "as-manufactured" state of the SiC-based CMC structure, several samples of the same material were polished (Fig.2b). All the samples were ultrasonic cleaned using methanol prior to the measurements.

2.1. Raman Spectroscopy

The Raman spectra were recorded at room temperature on a Horiba−Jobin−Yvon LabRAM HR confocal Raman microscope equipped with a Synapse CCD detector scanning area of 50 x 50 μm, using an excitation laser wavelength of 532 nm, operating at a power of $\sim$ 2 mW (10%) and a 1800 lines/mm grating. The Raman shift was calibrated using the Raleigh peak and the 520.7 cm^{-1} Silicon line from a Si(100) reference sample as previously done in the literature [29].

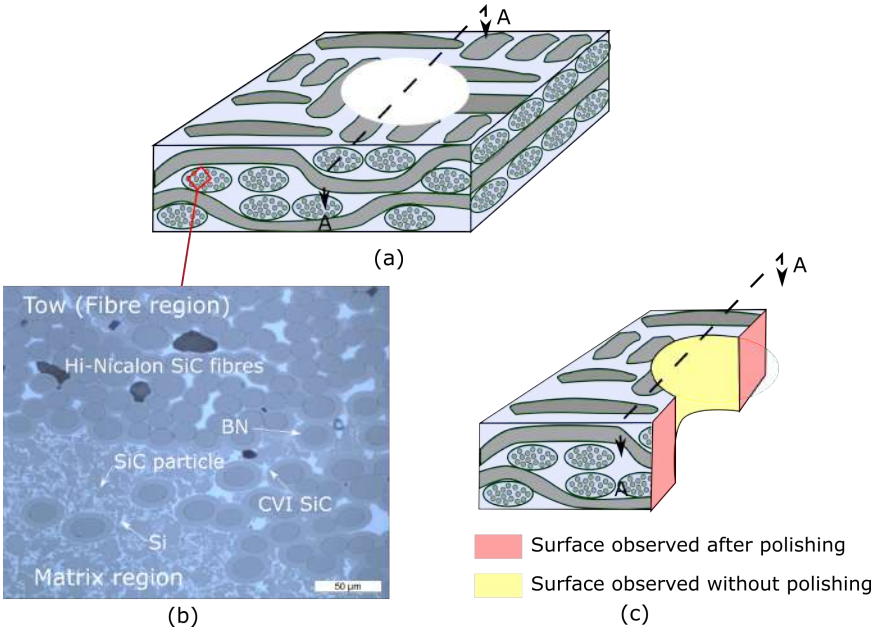

Figure 2: (a) Schematic of a CMC sample with a machined hole and showing (b) the microstructure of the "as-manufactured" CVI-MI SiC/SiC and (c) the "as-machined" surfaces to allow the evaluation of the damage induced by the machining, i.e. drilling process.

In the case of Hi-Nicalon fibres, the SiC structure contains a higher ratio of C to Si atoms [8], resulting in a dominant Carbon Raman spectrum. It has been previously reported [18] that degradation of Hi-Nicalon SiC fibres can be induced by the laser power, especially for power densities higher than approximately 1 mW/μm^2. In order to verify that this was not occurring, several tests have been carried out at lower power (0.25 μW scanning an area of 50 μm x 50 μm) and compared with the settings used for the results stated in this work, which revealed that degradation had not occurred at higher power densities.

As reported in the literature for Hi-Nicalon fibres [18, 30], when analysing the Raman spectra, a Lorentzian fitting for the carbon D peak (green) and Gaussian fittings for the carbon G (blue) and the D′ (red) peaks have been employed, as shown in Fig.3a. To characterise the fibre-rich regions, repeated (> 10) measurements (scanning an area of 50 x 50 μm^2) have been carried out on three different conditions:

(i) "Free fibres": separately delivered free tows without being embedded in a matrix

to measure the stress free conditions of the fibres.

(ii) "As-manufactured": tows which were embedded in the CMC matrix and after a polishing procedure, condition that enable the characterisation of the CVI-MI SiC matrix formation process.

(iii) "As-machined": tows which were embedded in the matrix and have been exposed to the machining process condition that enable the characterisation of the mechanical material removal process).

In the case of the SiC-Si matrix, the B-doped Si and the 6H-SiC peaks are found, producing the spectrum shown in Fig.3b. The B-doping changes the electronic structure of the Si producing non-symmetric peaks [31, 32] which are commonly fitted with a Fano line shape (Eq.1) [33]:

$$I(\omega) = I_0 \frac{(q+x)^2}{1+x^2} \quad where \quad x = \frac{\omega - \omega_0}{\tau} \tag{1}$$

where: I_0 - arbitrary intensity factor, q - the symmetry parameter, τ - width parameter and ω_0 - phonon wavenumber. As shown in Fig.3b, three fano-type peaks are found in the B-doped Si at 520 cm^{-1} (optical phonon), 620 cm^{-1} (B^{11}) and 644 cm^{-1} (B^{10}). On the other hand, the SiC particles showed the Raman spectrum typical from a 6H polytype with free-stress peaks at 767 cm^{-1}, 789 cm^{-1} and 797 cm^{-1} [34].

As aforementioned, residual stress information can be obtained from Raman Spectroscopy by addressing the peak shift. Knauf [19] presented the equations to convert the Raman peak shift ($\Delta\omega$) to hydrostatic residual stresses ($\Delta\sigma_H$) for Hi-Nicalon fibres, 6H-SiC particles and the free B-doped Si:

$$\begin{aligned} \Delta\sigma_{H,Hi-Nicalon} &= -0.333\Delta\omega \\ \Delta\sigma_{H,SiC} &= -0.283\Delta\omega \\ \Delta\sigma_{H,Si} &= -0.266\Delta\omega \end{aligned} \tag{2}$$

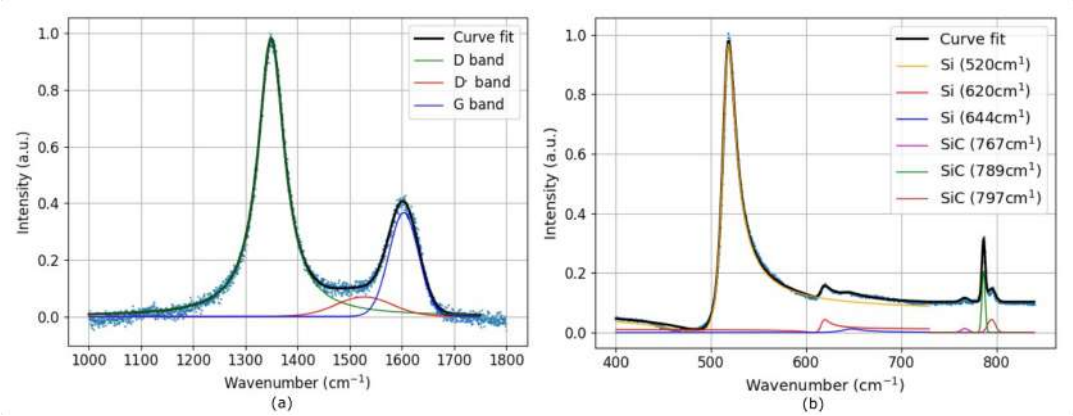

Figure 3: Raman spectra of (a) Hi-Nicalon SiC fibres with a Lorentzian fitting of the D peak (green) and Gaussian fitting of the G peak (blue) and D′ peak (red) with the resultant fitting plotted in orange; (b) SiC-Si matrix with three fano-line fitting peaks (Si) and the three Gaussian peaks (SiC).

2.2. Imaging analysis

To further understand the induced residual stresses and changes in chemical composition, qualitative information of the material removal mechanism by looking at the surface response was done via SEM and TEM. A Field Emission Gun SEM (JEOL 7100F FEG-SEM) was used to obtain high resolution information of the "as-manufactured" and "as-machined" state of the CMC. Afterwards, the subsurface from the "as-machined" samples was studied by preparing thin foils with a Focused Ion Beam (FIB) SEM (FEI Quanta200 3D DualBeam FIB/SEM) following the cross-sectional technique and thinning it up down to $\approx$ 150 nm, and were observed with TEM (JEOL 2100Plus) operated at 200 kV.

3. Results and discussion

From the machining point of view, slow tool (e.g. drill) feed rates are needed for the cutting of hard SiC-based CMCs to avoid the failure of the cutting tool [28]. This results in considerably small values of uncut chip thickness (≈ 1 μm) compared to either the fibre and matrix areas (≈ 200 μm), concluding that they are not simultaneously cut and therefore enabling their independent analysis. Hence, the following sections aim at explaining the material removal mechanism and capturing the induced damage displayed

by (i) the fibre-rich and (ii) the matrix-rich regions.

3.1. Machining induced damage within the fibre-rich region

3.1.1. Residual stresses and chemical composition

The Raman measurements performed on "as-manufactured" CMC samples show no statistically significant peak shift in the Carbon D peak (Fig.4a), matching previous results found in the literature for a similar CVI-MI SiC/SiC [19]. However, after the machining ("as-machined"), the fibres suffer a decrease in the D peak wavenumber which translates in tensile residual stresses. Using Eq.2, the hydrostatic residual stress induced during the machining process can then be calculated, i.e. 644 ± 225 MPa. The high standard deviation obtained for the "as-machined" samples, which is considerably larger compared to the "free fibres" and "as-manufactured", could be the outcome of non-constant thermal and mechanical loads occurring during the drilling of hard-heterogeneous materials such as SiC-based CMC [28]. The cutting phenomena behind the values of residual stresses are combined with the surface and subsurface analysis in the next section to provide an in-depth explanation of the material removal mechanism and surface damage.

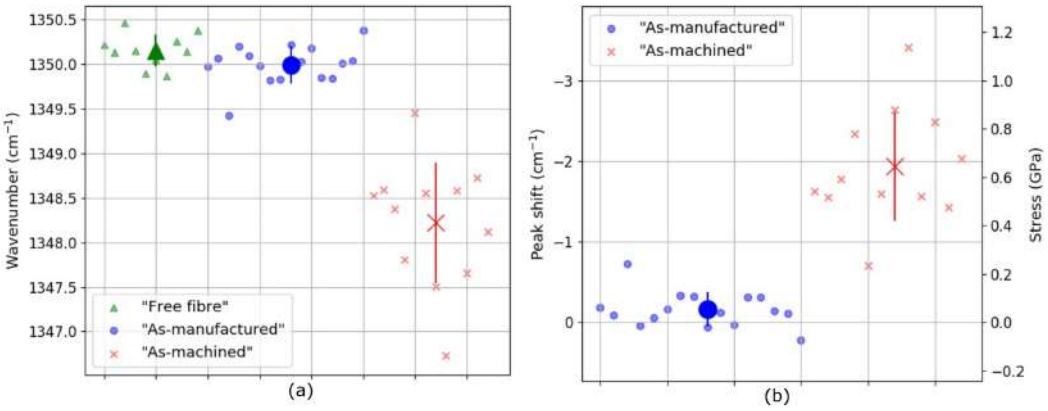

Figure 4: Raman spectroscopy results showing (a) the peak shift comparing the "free", "as-manufactured" and "as-machined" fibres and (b) the residual stresses obtained with Eq.2 for the "as-manufactured" and "as-machined" fibres, normalising the values with the average found for the "free" fibres. Data scatter of > 10 repeated measurements on areas of 50x50 μm

The Raman spectra found for the "as-manufactured" and "as-machined" samples do not display any significant change in terms of D/G peak ratio or bandwidth, meaning that

the fibres do not undergo any variation in terms of microstructure (e.g. crystallite size or amount of disorder in the C structure) nor in chemical composition (e.g. degradation or oxidation of the C).

Based on this set of analyses, it can be concluded that the machining process induces levels of tensile residual stress but no major changes in chemical composition are observed in the fibre-rich region. With this quantitative understanding of how the C domains in Hi-Nicalon fibres are strained as a result of the drilling loads, a study of the material removal mechanism by analysing the microstructure and morphology appearing in the "as-machined" surface is presented in the next section.

3.1.2. Understanding the material removal mechanism via microstructure evaluation of the affected surface

After the machining, the fibre-rich region shows evidence that the dominant material removal mechanism in drilling is brittle based, mainly with transgranular cleavage fracture (Fig.5).

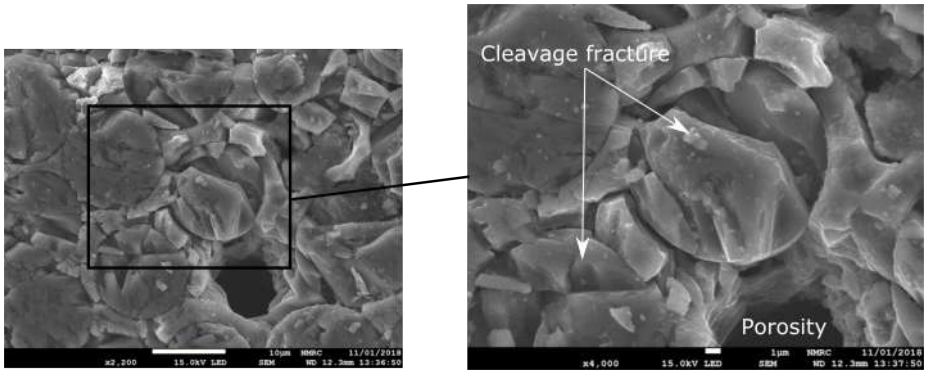

Figure 5: SEM image showing the transgranular cleavage fracture after the machining process in the fibre-rich region. NB: the pore observed is due to the manufacturing process (e.g. infiltration).

From the principles that govern the induction of residual stresses in cutting [35], it can be concluded that tensile residual stresses appear when the strain in the machined surface is primarily induced by the thermal load generated by the tool-workpiece friction. In this case it could be considered that, as brittle fracture is the dominating material removal mechanism, the mechanical-induced plastic flow absorbed by the material is limited and the main source of strain is of thermal nature. Fig.6 shows a simplified

schematic of the proposed material removal mechanism suffered by the fibres: when a thermal load is generated during cutting, the surface plastifies in compression (Fig.6a), leading to tensile residual stresses when it cools down (Fig.6b).

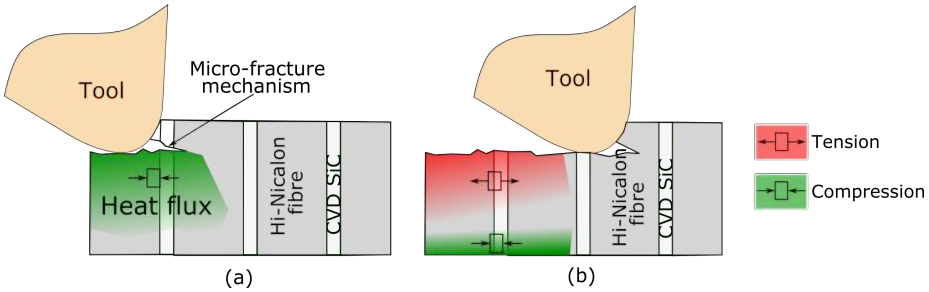

Figure 6: Schematic of the material removal mechanism showing (a) the effect of having a thermal load as a main source of material straining during cutting and (b) the resultant residual stresses found in the machined surface and subsurface.

It has been observed that after the machining, the CVI SiC coating of the fibres display a radial cracking (as shown in Fig.7 for two different fibres). A reason for the formation of these cracks could initially be related to the mismatch in coefficient of thermal expansion (CTE) between the Hi-Nicalon fibres and the CVI SiC coating. It is well known in the literature that CTE mismatch is a big challenge in CMCs, and in particular the case of these two materials, the CTE varies from 3.5 ppm/°C for the SiC Hi-Nicalon fibres to 4.5-5 ppm/°C for the CVI SiC [19, 36]. Nevertheless, the temperature expected during drilling of CMCs in the presence of coolant application is less than the peak processing temperature that these materials are exposed to, which is around 1400 °C [19]. Therefore, the origin of the radial fracture found in the CVI SiC structure should be linked to the mechanical load applied during the machining process; however, this radial nature of cracking will be further investigated.

To further validate the chemical analysis concluded with Raman spectroscopy and in order to better understand how the material fractures by interpreting the microstructure and morphology of the CVI SiC coating, a TEM study of a region including a Hi-Nicalon fibre, a CVI BN and a CVI SiC coating is presented in Fig.8. It can be observed that, while the Hi-Nicalon fibres show a nanocrystalline structure, the CVI SiC coating has columnar preferential grain growth (which expands radially from the fibre surface) and

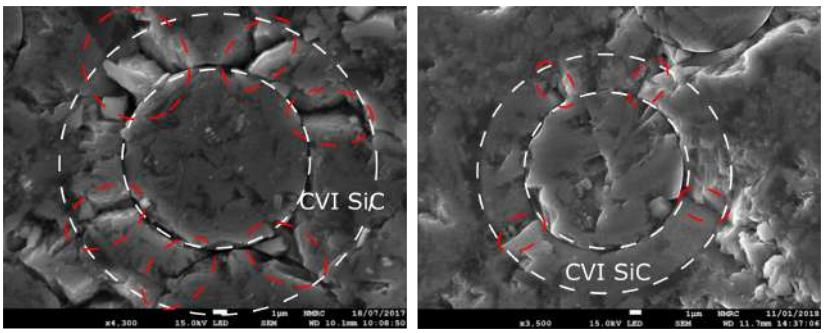

Figure 7: Two examples of the machined surface in the fibre-rich region showing the formation of radial cracks in the CVI SiC coating surrounding the fibres.

that the radial fracture follows this intercolumnar direction, which is the weakest fracture plane. Hence, the specific fracture mode appearing in cutting is affected by the CVI growing structure leading to a unique signature on the machined surface.

Electron energy loss spectroscopy (EELS) was performed in a Hi-Nicalon fibre from the machined surface to the subsurface. The graphitic and amorphous Carbon signature did not show any considerable change, confirming the conclusions drawn from Raman spectroscopy using the bandwidth of the D peak and the D-G peak ratio analysis. Moreover, the EDS spectra showed that no significant increase in oxygen content is found at the surface but only on the material that has filled the fractured area (called fractured material in Fig.8b), concluding that in the machined surface of the fibre-rich region, no C or SiC oxidation occurs.

Due to the orthotropic nature of long-fibre reinforced materials such as CMCs, two main fibre orientations are faced by the cutting tool (see Fig.1). So far in this study, only transverse fibres have been studied as their surface integrity is more challenging to characterise (i.e. they are exposed to more complex fracture mechanisms). On the other hand, the material removal mechanism appearing for longitudinal fibres is based on a debonding action leading to a surface with pull or unpulled fibres and with a minority of them begin fractured along its longitudinal axis (Fig.9).

The phenomenon characterising the material removal mechanism in the fibre-rich region has been explained based on the tensile residual stresses and the morphology of the fracture-dominated evidence found in the machined surface. In the next section, a

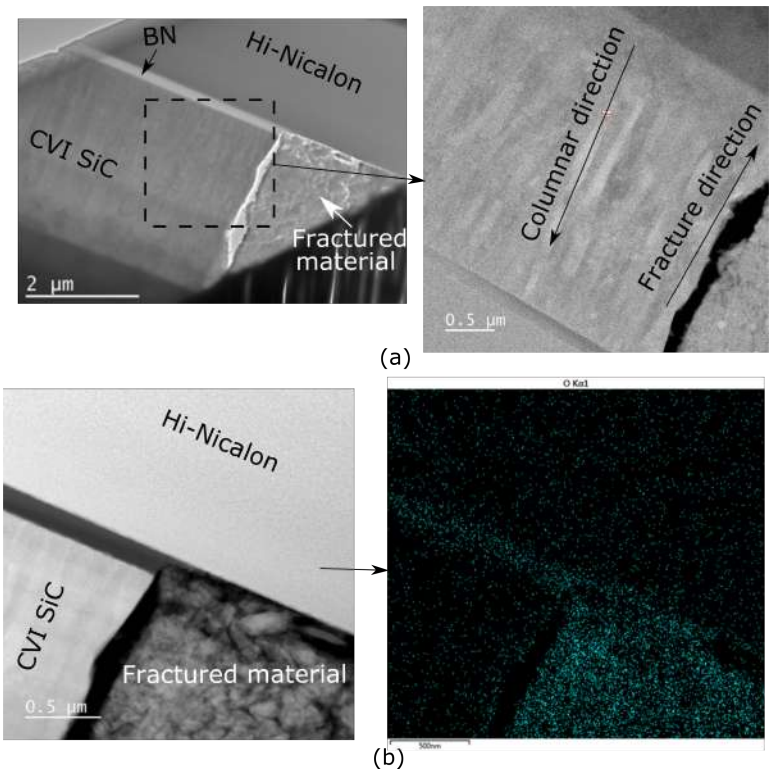

Figure 8: TEM analysis of a region including a Hi-Nicalon fibre, a CVI BN and CVI SiC coating (a) BF TEM image of the fracture mechanism suffered by the SiC columnar structure; (b) STEM analysis and EDS signal showing a greater concentration of oxygen in the fractured material.

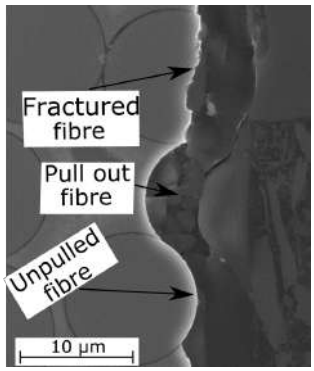

Figure 9: Three cutting mechanisms found in a single sample region when cutting longitudinal fibres (placed parallel to the cutting direction, Fig. 1a): fractured, pull-out and unpulled fibre

detailed explanation of the behavior presented by the matrix-rich region during machining utilising the above procedures is presented.

3.2. Machining induced damage within the matrix-rich region

3.2.1. Residual stresses and chemical composition

Following the strategy defined by Knauf [20] to calculate the residual stresses in a B-doped Si with a non-constant concentration, a stress free line which considers the peak half width (as an indicator of the B concentration) and the wavenumber of the 520 cm^{-1} peak has been plotted with a black line in Fig.10a. It can be observed that initially ("as-manufactured") the Si appears slightly under compression which shows a comparable tendency with the results from the literature [19]. However, back to back values should not compared because in the current work a different laser wavelength is used (532 nm in the current work instead of 515 nm [31, 19]) and this can slightly influence the results. Nevertheless, as the main objective of this work is to enable deeper understanding of the effect of machining on CMC structures, the values of peak shift have been normalised by the "as-manufactured" average. It can be observed from Fig.10b that between the "as-manufactured" and the "as-machined" samples there is a variation in peak shift corresponding to 316 $\pm$ 117 MPa of residual stresses in compression. However, in specific regions of the CMCs, the Raman peak shift seems to suffer a greater drop (green squares) which is directly related to a variation in the Raman spectrum.

Analysing these zones in further detail, it is observed that only specific regions of the Si matrix tend to suffer a transformation in the Raman spectra where a peak starts to appear below 500 cm^{-1} (as shown in Fig.11a). This alteration in the Raman spectra can be related to an amorphisation of the Si [37] that due to the high strain and temperature applied during the machining process leads to a redeposition of melted Si on the machined surface (see Fig.11b).

The Raman peak shift and the stress conversion of the 789 cm^{-1} peak found in the 6H-SiC particles is shown in Fig.12. It can be seen that initially ("as-manufactured") the SiC particles are under tensile residual stresses, as presented in the literature [19]. However, after machining a reduction in the peak shift is observed, resulting in a decrease of tensile stresses (either inducing compressive or releasing tensile stresses). Nevertheless, the

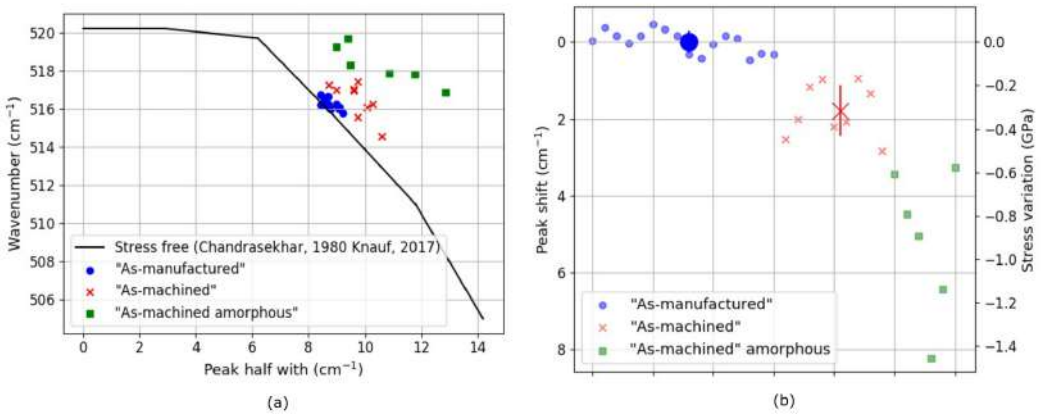

Figure 10: Raman spectroscopy results from the B-doped Si using (a) a stress free line in a wavenumber vs peak half width plot and (b) peak shift (left scale) and stress variation (right scale) using Eq.2 and normalising for the 'as-manufacturing' average.

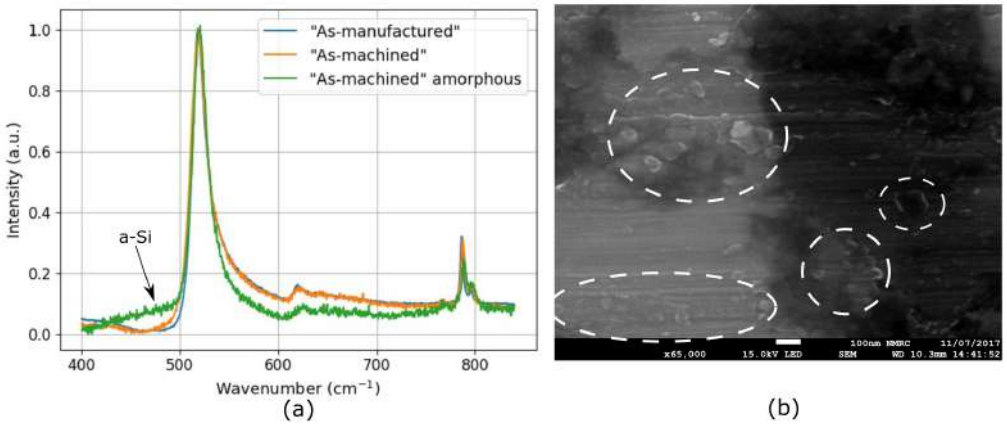

Figure 11: (a) Raman spectra of three different measurements of the B-doped Si: "as-manufactured", "as-machined" and "as-machined" amorphous; (b) SEM image of the matrix region showing some evidence of redeposited material on the machined surface (scale 100 nm).

variation in peak shift is small and with large values of standard deviations, questioning the statistical significance of the determined results.

The main reason for the difference in values found for the SiC could be related to the penetration depth of the laser used for the Raman measurements. Due to the different light absorption coefficient of each constituent of SiC-based CMCs, the penetration depth for Si and C remains considerably smaller than 1 μm while for SiC the order of

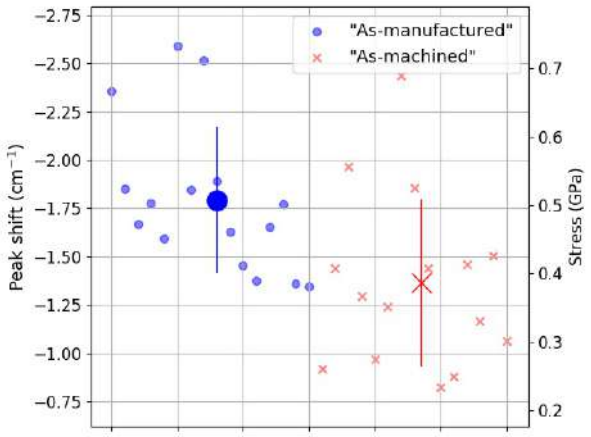

Figure 12: Peak shift and residual stress conversion (calculated with Eq.2) obtained for the 789 cm^{-1} stress-free peak appearing in the 6H-SiC Raman spectra.

magnitude is 1000 times greater (around 700 μm) [19, 38]. The higher penetration depth presented by the SiC particles leads to a measurement where the subsurface is also analysed, adding non-affected SiC particles to the measurement and which is translated into greater standard deviations. In their work, Ghosh et al. [26] claimed to be able to calculate surface residual stresses induced by a scratch test on the SiC particles reinforcing a ZrB_2 matrix. Because of the lower concentration of SiC particles (5%), this measurement might have been more accurate, however, in the case of a SiC/SiC, the amount of SiC particles forming the MI-CMC matrix is considerably higher (as shown in Fig.2b) and the measurements can then be affected.

Hence, it can be concluded that compressive residual stresses are induced to the Si regions and specific areas might experience an amorphisation which has been associated with a redeposition of melted Si (Fig.11) during machining. Moreover, the SiC particles also tend to suffer an increase in peak shift which translates in compressive or release of tensile residual stresses. Nevertheless, because of the higher laser penetration depth in the SiC, Raman spectroscopy should not be used to quantify the results but just to present the tendency behind the material removal process. An in-depth understanding of the material removal mechanism and surface damage is presented in the next section.

3.2.2. Understanding the material removal mechanism via microstructure evaluation

In contrast with the results found in the fibre-rich region, when machining the matrix, the material tends to suffer a ductile behaviour with some particles being pull-out (Fig.13), as similarly reported for the analysis of a reaction bonded SiC surface after grinding with small uncut chip thickness [39].

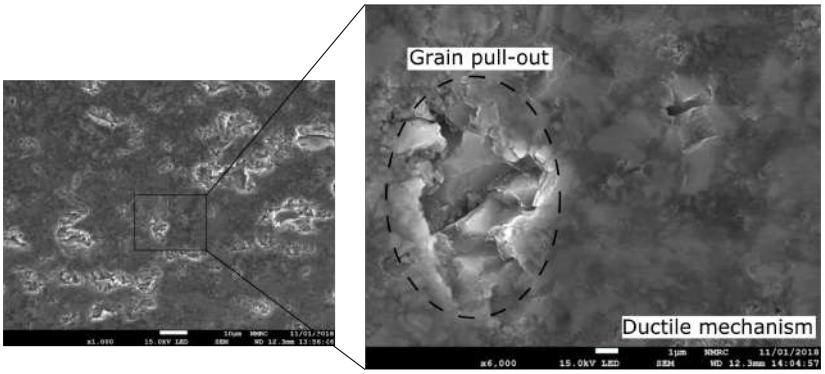

Figure 13: Machined surface from a normal view showing evidence of the ductile behaviour and grains pull-out in the SiC-Si matrix.

In this case, the removal mechanism occurring ahead of the cutting edge is based on localised plastic deformation which induces a stress field into the material (Fig.14a). Therefore, corroborating the compressive residual stresses found with the Raman analysis and the evidence of plastic deformation found in the machined surface, it could be concluded that the SiC-Si machined surface is mainly generated by a mechanic induced plastic strain. This conclusion is in good agreement with the principles of residual stresses upon cutting where compressive residual stresses are found in the surface when a mechanical-induced strain is the dominating removal mechanism. This phenomenon has been schematically represented in Fig.14, where the material is subject to a directional stress field in the cutting direction which compresses the surface found ahead of the cutting edge and consequently pulls the material behind (see Fig.14a). Hence, when the tool moves away, as the material has plasticised in a tensile state, compressive residual stresses are found in the surface. (Fig.14b).

To further understand the material removal process, the subsurface of an area including a 6H-SiC particles and free Si was analysed in cross section with TEM. Fig.15a

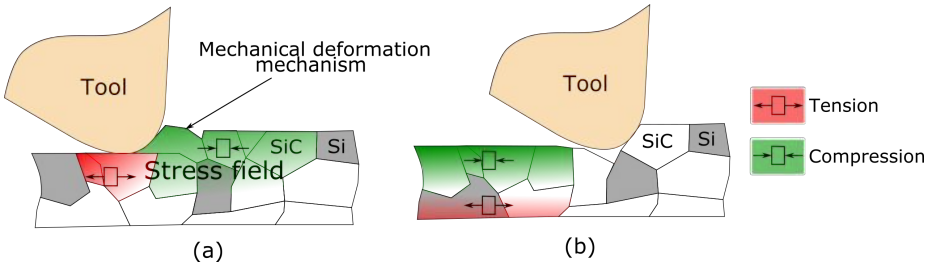

Figure 14: Schematic of the material removal mechanism showing (a) the effect of having a mechanical load as a main source of material straining during cutting and (b) the resultant residual stresses found in the machined surface and subsurface.

and Fig.15b show how a $\approx$ 1 μm layer of the SiC-Si material is mechanically affected by strain and fracture. The EDS analysis of the fracture site shows how the crack does not follow the SiC-Si interfaces producing trans-particle fracture. Moreover, oxidation of the non-oxide ceramics (i.e. SiC and Si) is just observed in the crack paths and it is difficult to conclude if it is caused by the FIB milling process or because of infiltration of coolant during the machining. Nevertheless, in the case of SiC/SiC CMCs, an obvious recrystallization layer (known as white layer [23] when found in refractory metals such as Nickel-based alloys) is not formed after the machining process.

3.3. Influence of the composition, microstructure and morphology of SiC-based materials upon cutting

During the cutting of CVI-MI SiC/SiC CMC, three different SiC-based materials are encountered by the cutting edge (cut at the same conditions) observing distinct material removal mechanisms for each as follows:

- The Hi-Nicalon fibres are formed by a 3C-SiC polytype with a nanocrystalline grain structure (grain size, $d_{size} \approx$ 10 nm) and with free turbostatic Carbon [40] (Fig. 16a). As shown in Fig.5, this structure presented a tendency of being removed by a brittle transgranular cleavage fracture.

- The SiC particles found in the SMI matrix are formed by a 6H-SiC polytype with a microcrystalline structure (grain size, $d_{size} \approx$ 1-2 μm, Fig.16b). These particles tended to display a dominating ductile deformation mechanism. In some cases, the particles were fractured and pulled out from the matrix (see Fig.13).

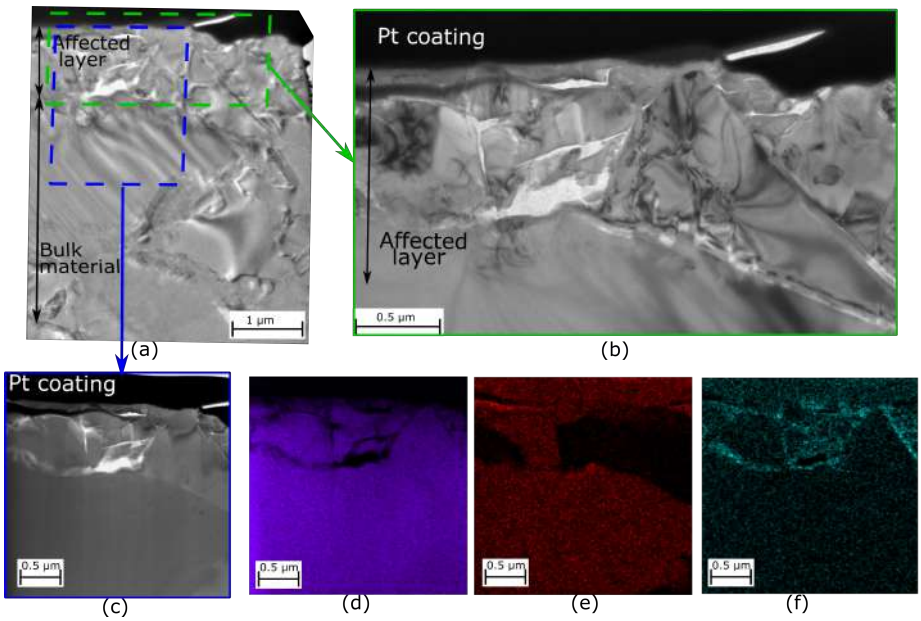

Figure 15: TEM analysis of the matrix-rich region showing (a) and (b) via BF TEM the thickness of the affected layer, (c) BF STEM of the affected region with an EDS analysis showing the concentration of (d) Silicon, (e) Carbon and (f) Oxygen.

- The CVI SiC coating surrounding the fibres is formed by ultrafine and elongated grains (grain size, $d_{size} \approx 100$ nm, Fig.16c). The coating showed a tendency to radial fracture which was related to the columnar growth of the CVI process (see Fig.7).

It has been reported in the literature that brittle materials can undergo a ductile-to-brittle (DTB) transition when cutting. This transition depends on the energy required for the material to attain plastic flow (E_p) and fracture (E_f). This can be analytically formulated as [41]:

$$DTB \propto \frac{E_p}{E_f} = \frac{\sigma_y V_p}{G A_f} \tag{3}$$

with σ_y - yield strength, V_p - volume of material being deformed, G - energy release rate and A_f - fractured area. Assuming that V_p and A_f are proportional to the characteristic length of material being removed (i.e. $V_p \approx d^3$ and $A_f \approx d^2$), for a given material the DTB transition is proportional to d, which in a cutting scenario is translated to the

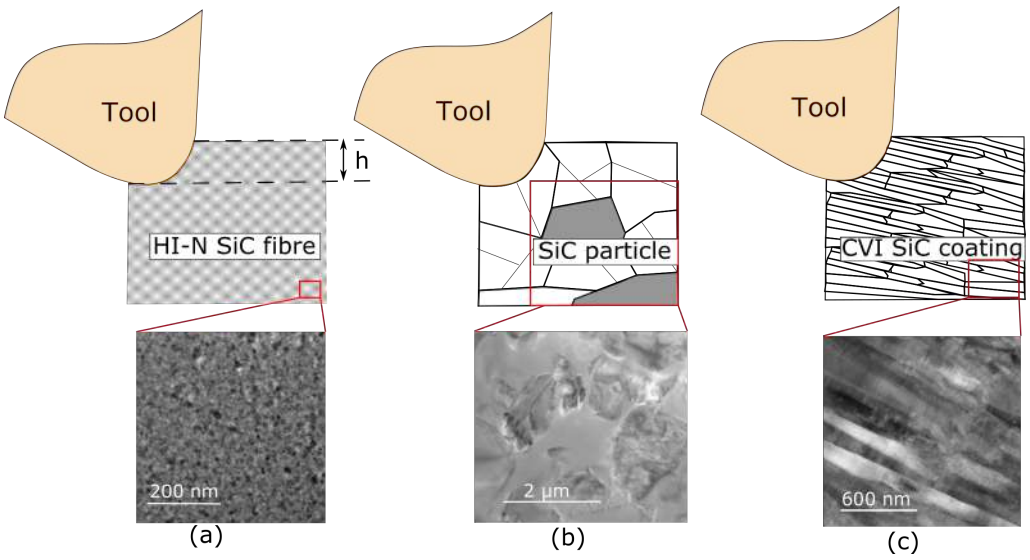

Figure 16: Effect of cutting on different SiC-based constituents of the CMC (a) Hi-Nicalon fibre containing nanocrystalline 3C-SiC and turbostatic Carbon, (b) polycrystalline 6H-SiC particles and (c) CVI coating with a columnar structure.

uncut chip thickness (h_d) [41]:

$$DTB \propto \frac{\sigma_y V_p}{G A_f} \propto h_d \tag{4}$$

Nevertheless, when cutting the different constituents found in the CVI-MI SiC/SiC CMC structure, the uncut chip thickness (h_d) is constant for each of them and hence the DTB transition must come from the different material responses (i.e. intrinsic material properties defined by the microstructure, morphology and chemical composition). From linear elastic fracture mechanics, the fracture toughness of a material can be related to the energy release rate as:

$$G \propto K_{ic} \propto \sigma\sqrt{\pi a_{cri}} \tag{5}$$

with K_{ic} - fracture toughness, σ - stress and a_{cri} - critical flaw size for the the crack to propagate. Because of the different microstructure between the SiC-based materials, the critical flaw size varies and in crystalline ceramics this can be analytically defined as $a_{cri} = 2\mathrm{d}_{size}$ [42]. In cutting, small values of material are interacting with the cutting

edge - defined by the uncut chip thickness (h_d) - that when drilling with a standard twist drill can be analytically calculated as [43]:

$$h_d = f_z sin\varphi = \frac{f}{v} sin\varphi \approx 1\mu m \tag{6}$$

with f_z - feed per tooth and φ - half of the drill point angle.

Hence, two main scenarios should be defined based on the grain size of the material and the uncut chip thickness:

- If the grain size is small compared to the uncut chip thickness ($d_{size} < h_d$) at each instant of the cutting process several defects (defined by a_{cri}) are encountered by the cutting edge, leading to a fracture dominated removal process.
- If the grain size is large compared to the uncut chip thickness ($d_{size} > h_d$) the cutting edge is likely to, for the majority of cutting instants, not find defects in the structure, leading to a ductile dominated removal process.

Hence, this explains why the Hi-Nicalon fibres ($d_{size} \approx$ 10 nm) and the CVI SiC ($d_{size} \approx$ 100 nm) tend to undergo a fracture dominated removal mechanism when drilling with a $h_d \approx 1$ μm. On the other hand, the grain size of the SiC particles ($d_{size} \approx$ 1-2 μm) is within the same magnitude as the uncut chip thickness resulting in a more ductile removal. Furthermore, this tendency is in good agreement with the Hall-Petch relationship [42], that by using the equations for yield stress (σ_y) and cleavage stress (σ_c), the DTB transition could be defined as:

$$DTB \propto \frac{\sigma_0 + k_y d_{size}^{-1/2}}{\sigma_{0c} + k_c d_{size}^{-1/2}} \tag{7}$$

where σ_0 is the friction stress required to move dislocations and σ_{0c} is the stress required to start the cleavage fracture. Knowing that $k_c > k_y$ [42] it can be concluded that the DTB will have a inverse relation with the grain size - i.e. the material will tend to suffer a brittle behaviour for small grain sizes.

Aside from the microstructure, the morphology and chemical composition can also play an important role in the DTB transition when cutting SiC-based materials:

- The turbostatic C found in the Hi-Nicalon fibres can be seen as a source of defects and inclusions which decreases the tendency of the 3C-SiC grains to plastically deform.

- The columnar growth of the CVI SiC produces an anisotropic fracture toughness with weaker interfaces almost aligned with the cutting direction (see Fig.16c).

Thus, the microstructure, morphology and chemical composition of SiC materials dominate the material removal process leading to different DTB transition which has been shown of high relevance for the surface integrity.

4. Conclusions

In the present study, the microstructure of the machined surface of a long fibre reinforced CMC (in this study a CVI-MI SiC/SiC) has been characterised, by explaining the material removal mechanism and by capturing the associated surface damage. The main contributions of this work are:

- The plastic strain induced in the surface during the severe mechanical and thermal loads generated by the cutting process has been characterised for the first time by using Raman Spectroscopy and obtaining tensile residual stresses in the fibre-rich areas and compressive in the matrix-rich areas. The Raman signature also allowed an understanding of the elemental distribution within the heterogeneous structure, concluding that some amorphous Silicon is redeposited in the surface.

- The material removal mechanism has been understood by characterisation techniques (via a FEG-SEM) of the microstructure found in the affected surface. This showed clear evidence that the fibres suffer a brittle fracture-dominated behaviour while the matrix region suffered a plastic-dominated mechanism with some SiC particles being pull-out (debonding mechanism).

- Using the fundamentals of residual stresses upon cutting it can be concluded that in the fibre region, because of the dominating brittle fracture behaviour and the tensile residual stresses measured, the main source of strain is induced via a heat stress gradient. On the other hand, in the matrix region, the evidence of plastic

deformation together with the compressive residual stresses conclude that the main strain source is of mechanical nature.

- TEM analysis of the CVI SiC coating showed how its columnar structure influences the fracture mechanism suffered during machining by a preferential intercolumnar fracture direction. The origin of this fracture has been attributed to the mechanical load, as even the CTEs mismatch, the cutting temperature reached during a coolant-assisted machining process should be considerably lower than the peak temperature experienced by the material during the manufacturing process (e.g. melt infiltration or post heat treatments).

- A TEM analysis characterising both materials (i.e. Si and SiC) found in the matrix region has been presented showing an affected (strained and fractured) layer of around 1 μm. From the EDS analysis, the fracture has been shown to not follow the SiC-Si interfaces.

- Different material removal mechanisms when cutting at the same conditions have been observed for the different SiC-based materials found in the CMC structure (i.e. Hi-Nicalon fibres, CVI coating and SiC particles). This has been analytically explained based on how the ductile to brittle transition is affected by the microstructure and also linked to the morphology and chemical composition of each SiC-based material.

Acknowledgements

The authors gratefully acknowledge Rolls Royce Plc for the funding support received during the work. The facilities used for this research work were from the Nanoscale and Microscale Research Centre (NMRC) at the University of Nottingham.

References

[1] James A. DiCarlo. Advances in SiC/SiC Composites for Aero-Propulsion. In *Ceramic Matrix Composites*, pages 217–235. John Wiley & Sons, Inc., Hoboken, NJ, USA, oct 2014.

[2] Bernhard Heidenreich. C/SiC and C/C-SiC Composites. In *Ceramic Matrix Composites*, pages 147–216. John Wiley & Sons, Inc., Hoboken, NJ, USA, oct 2014.

[3] Paolo Colombo, Gabriela Mera, Ralf Riedel, and Gian Domenico Soraru. Polymer-derived ceramics: 40 Years of research and innovation in advanced ceramics. *Journal of the American Ceramic Society*, 93(7):1805–1837, 2010.

[4] See Hoon Lee, Markus Weinmann, and Fritz Aldinger. Processing and properties of C/Si-B-C-N fiber-reinforced ceramic matrix composites prepared by precursor impregnation and pyrolysis. *Acta Materialia*, 56(7):1529–1538, 2008.

[5] Kent J. Probst, Theodore M. Besmann, David P. Stinton, Richard A. Lowden, Timothy J. Anderson, and Thomas L. Starr. Recent advances in forced-flow, thermal-gradient CVI for refractory composites. *Surface and Coatings Technology*, 120-121:250–258, 1999.

[6] Jacques Lamon. Chemical Vapor Infiltrated SiC/SiC Composites (CVI SiC/SiC). In Narottam P. Bansal, editor, *Handbook of Ceramic Composites*, chapter 3, pages 55–76. Kluwer Academic Publishers, 2005.

[7] G. S. Corman and K. L. Luthra. Silicon Melt Infiltrated Ceramic Composites (HiPerComp^{TM}). In Narottam P. Bansal, editor, *Handbook of Ceramic Composites*, chapter 5, pages 99–115. Kluwer Academic Publishers US, 2005.

[8] A. R. Bunsell and A. Piant. A review of the development of three generations of small diameter silicon carbide fibres. *Journal of Materials Science*, 41(3):823–839, 2006.

[9] Bradley L. Wing and John W. Halloran. Microstress in the Matrix of a Melt-Infiltrated SiC/SiC Ceramic Matrix Composite. *Journal of the American Ceramic Society*, 38(1):42–49, 2017.

[10] S Bertrand, C Droillard, R Pailler, X Bourrat, and R Naslain. TEM structure of (PyC/SiC). *Journal of the European Ceramic Society*, 20:1–13, 2000.

[11] J. J. Brennan. Interfacial characterization of a slurry-cast melt-infiltrated SiC/SiC ceramic-matrix composite. *Acta Materialia*, 48(18-19):4619–4628, 2000.

[12] J Pailler, Jacques L Lamon, and Roger R Naslain. Single- and Multilayered Interphases in SiC / SiC Composites Exposed to Severe Environmental Conditions : An Overview. *Applied Ceramic Technology*, 275:263–275, 2010.

[13] Nasrin Al Nasiri, Niranjan Patra, Na Ni, Daniel D. Jayaseelan, and William E. Lee. Oxidation behaviour of SiC/SiC ceramic matrix composites in air. *Journal of the European Ceramic Society*, 36(14):3293–3302, 2016.

[14] J. A. DiCarlo, H M. Yun, G. N. Morscher, and R. T. Bhatt. SiC/SiC Composites for 1200 \degree C and Above. In Narottam P. Bansal, editor, *Handbook of Ceramic Composites*, chapter 4, pages 77–98. Kluwer Academic Publishers, 2005.

[15] C Galiotis. A study of mechanism of stress transfer in continous- and discontinous-fibre model composites by laser raman spectroscopy. *Composites Science and Technology*, 48:15–28, 1993.

[16] Phillip Jannotti, Ghatu Subhash, James Zheng, and Virginia Halls. Measurement of microscale residual stresses in multi-phase ceramic composites using Raman spectroscopy. *Acta Materialia*, 129:482–491, 2017.

[17] Bradley L Wing. *Residual Stresses and Oxidation of Silicon Carbide Fiber Reinforced Silicon Carbide Composites*. PhD thesis, University of Michigan, 2016.

[18] Gwenael Gouadec, Philippe Colomban, and Narottam P Bansal. Raman study of Hi-Nicalon-fiber-reinforced celsian composites: II, Residual stress in fibers. *Journal of the American Ceramic Society*, 84:1136–1142, 2001.

[19] Michael W. Knauf. *Effects of heat treatment in SiC/SiC Ceramic Matrix Composites*. PhD thesis, Purdue University, 2017.

[20] Michael W Knauf, Craig P Przybyla, Andrew J. Ritchey, Rodney W Trice, and R Byron Pipes. Residual Stress Determination of Silicon Containing Boron Dopants in CMCs. *Journal of the American Ceramic Society*, 2018.

[21] J. G. Li, M. Umemoto, Y. Todaka, and K. Tsuchiya. A microstructural investigation of the surface of a drilled hole in carbon steels. *Acta Materialia*, 55(4):1397–1406, 2007.

[22] Rachid M'Saoubi, Dragos Axinte, Christopher Herbert, Mark Hardy, and Paul Salmon. Surface integrity of nickel-based alloys subjected to severe plastic deformation by abusive drilling. *CIRP Annals - Manufacturing Technology*, 63(1):61–64, 2014.

[23] Zhe Chen, Magnus Hörnqvist Colliander, Gustav Sundell, Ru Lin Peng, Jinming Zhou, Sten Johansson, and Johan Moverare. Nano-scale characterization of white layer in broached Inconel 718. *Materials Science and Engineering A*, 684(September 2016):373–384, 2017.

[24] Jiwang Yan, Zhiyu Zhang, and Tsunemoto Kuriyagawa. Mechanism for material removal in diamond turning of reaction-bonded silicon carbide. *International Journal of Machine Tools and Manufacture*, 49(5):366–374, 2009.

[25] Dipankar Ghosh, Ghatu Subhash, Ramachandran Radhakrishnan, and Tirumalai S. Sudarshan. Scratch-induced microplasticity and microcracking in zirconium diboride-silicon carbide composite. *Acta Materialia*, 56(13):3011–3022, 2008.

[26] Dipankar Ghosh, Ghatu Subhash, and Nina Orlovskaya. Measurement of scratch-induced residual

stress within SiC grains in ZrB2-SiC composite using micro-Raman spectroscopy. *Acta Materialia*, 56(18):5345–5354, 2008.

[27] D.A Axinte O Gavalda Diaz. Towards understanding the cutting and fracture mechanism in ceramic matrix composites. *International Journal of Machine Tools and Manufacture*, 118-119(March):12–25, 2017.

[28] O Gavalda Diaz, D A Axinte, and D Novovic. Probabilistic modelling of tool unbalance during cutting of hard- heterogeneous materials : A case study in Ceramic Matrix Composites (CMCs). *Composites Part B*, 148(March):217–226, 2018.

[29] Akos Botos, Johannes Biskupek, Thomas W. Chamberlain, Graham A. Rance, Craig T. Stoppiello, Jeremy Sloan, Zheng Liu, Kazutomo Suenaga, Ute Kaiser, and Andrei N. Khlobystov. Carbon Nanotubes as Electrically Active Nanoreactors for Multi-Step Inorganic Synthesis: Sequential Transformations of Molecules to Nanoclusters and Nanoclusters to Nanoribbons. *Journal of the American Chemical Society*, 138(26):8175–8183, 2016.

[30] G Gouadec and Ph Colomban. Micro-Raman stress imaging of ceramic (C , SiC) -fiber-reinforced ceramic-matrix and metal – matrix composites. *Materials Science and Engineering A*, 288:132 – 137, 2000.

[31] M. Grimsditch Meera Chandrasekhar, H. R. Chandrasekhar and M. Cardona. Study of the localized vibrations of boron in heavily doped Si Meera. *Physcal Review B*, 22(10):4825–4833, 1980.

[32] N H Nickel, P Lengsfeld, and I Sieber. Raman spectroscopy of heavily doped polycrystalline silicon thin films. *Phys. Rev. B*, 61(23):558–561, 2000.

[33] F. Cerdeira, T. A. Fjeldly and M. Cardona. Raman study of the interaction between localized vibrations and electronic excitations in boron-doped silicon. *Physical Review B*, 9(10):4344, 1974.

[34] S. Nakashima and H. Harima. Raman Investigation of SiC Polytypes. *Physica Status Solidi A*, 162:39–64, 1997.

[35] S. Valette J. Rech, H. Hamdi. Workpiece surface integrity. In P. Davim, editor, *Machining : fundamentals and recent advances*, chapter 3, pages 59–96. Springer, 2008.

[36] Yutai Katoh, Kazumi Ozawa, Chunghao Shih, Takashi Nozawa, Robert J. Shinavski, Akira Hasegawa, and Lance L. Snead. Continuous SiC fiber, CVI SiC matrix composites for nuclear applications: Properties and irradiation effects. *Journal of Nuclear Materials*, 448(1-3):448–476, 2014.

[37] Jiwang Yan, Tooru Asami, and Tsunemoto Kuriyagawa. Nondestructive measurement of machining-induced amorphous layers in single-crystal silicon by laser micro-Raman spectroscopy. *Precision Engineering*, 32(3):186–195, 2008.

[38] A C Ferrari and J Robertson. Resonant Raman spectroscopy of disordered , amorphous , and diamondlike carbon. *PHYSICAL REVIEW B*, 64(July):1–13, 2001.

[39] Jianbo Dai, Honghua Su, Tengfei Yu, Hao Hu, Wenbo Zhou, and Wenfeng Ding. Experimental investigation on materials removal mechanism during grinding silicon carbide ceramics with single diamond grain. *Precision Engineering*, 51(April 2017):271–279, 2018.

[40] A. R. Bunsell and M. H. Berger. Fine diameter ceramic fibres. *Journal of the European Ceramic Society*, 20(13):2249–2260, 2000.

[41] T. G. Bifano, T. A. Dow, and R. O. Scattergood. Ductile-Regime Grinding: A New Technology for Machining Brittle Materials. *Journal of Engineering for Industry*, 113(2):184, 1991.

[42] K. Chawla M. Meyers. Fracture: Microscopic Aspects. In *Mechanical behavior of Materials*, chapter 8, pages 466–524. Cambridge, 2nd edition, 2009.

[43] Viktor P. Astakhov. *Drills : science and technology of advanced operations*. 2010.